Modelling of longwave radiation exchange at greenhouse surfaces under all-sky conditions

Erick Kiplangat Ronoh[1*], Thomas Rath[2]

(1. Biosystems Engineering Section, Institute of Horticultural Production Systems, Leibniz Universität Hannover, Hannover, Germany; 2. Biosystems Engineering Laboratory, University of Applied Sciences Osnabrück, Osnabrück, Germany)

Abstract: Accurate and detailed longwave radiation heat transfer models are necessary in modern protected cultivation especially for greenhouses. For this reason, the study focuses on modelling the longwave radiation exchange between glass-covered greenhouse surfaces and the sky taking into consideration representative test conditions. Apart from the surface design and the thermal properties of the cover, the key meteorological parameters influencing longwave radiation models include air temperature, cloudiness and relative humidity. To model the downwelling longwave radiation under all-sky conditions, an effective atmospheric emissivity is required, which depends on the cloudiness of the sky. To achieve this, 10 typical clear-sky atmospheric emissivity equations were selected from the literature and their performances assessed. From comparative statistics, the Sugita and Brutsaert (1993) model produced the best results for emissivity estimations both at night and during the day. To work with the model a cloudiness factor was derived from analyzed weather maps and with the cloudiness octa (eighth) assigned by weather watchers. The best simulation results for both the downwelling and the upwelling longwave radiation were obtained with the map-based cloudiness factor. However, the errors related to the model performance with the two cloudiness prediction approaches were not significantly different. The thermal emissions were weighted according to the computed view factors and these enhanced delivery of reliable results in the simulation models. The most sensitive parameters in the longwave radiation models were found to be the air temperature and the surface-to-air temperature difference (sensitivity index SI > 1). Furthermore, the SI of the models with respect to the cloudiness was always higher than that with respect to the relative humidity. Overall, precise measurement or estimation of atmospheric parameters is important in accurate modelling of the exterior longwave radiation exchange.

Keywords: modelling, radiation exchange, greenhouse surface, sky

Citation: Ronoh, E. K., and T. Rath. 2015. Modelling of longwave radiation exchange at greenhouse surfaces under all-sky conditions. Agric Eng Int: CIGR Journal, 17(4):23-35.

1 Introduction

Longwave radiation exchange is an important factor in the thermal modelling of greenhouses. Thus, knowledge of the longwave radiation exchange is important for numerous applications in agriculture requiring surface radiation and energy balance. Detailed radiation models for the thermal exchange between the exterior surfaces of buildings and the surroundings are necessary to calculate energy balances on the exterior surface (Romila, 2012). The net heat exchange between two surfaces is dependent on their surface temperatures, relative areas and positions, and surface properties such as emittance and transmittance (Evins et al., 2014). Longwave radiation could be separated into downwelling and upwelling radiation. Downwelling radiation is the thermal radiation emitted by the atmosphere downward to the ground surface. An accurate prediction of this radiation from the sky is needed for many fields in agriculture, ranging from calculation of building energy requirements to estimation of climate change. Upwelling longwave radiation is the thermal radiation emitted by surfaces (it includes also the reflected atmospheric longwave radiation).

Generally, the longwave radiative exchange occurs between exterior building surfaces and elements which

Received date: 2015-07-12 Accepted date: 2015-08-26

***Corresponding author: Erick K. Ronoh,** Biosystems Engineering Section, Institute of Horticultural Production Systems, Leibniz Universität Hannover, Herrenhäuser Str. 2, D-30419 Hannover, Germany. Email: ronoh@bgt.uni-hannover.de; eriqueron2002@yahoo.com

include sky, ground and other surfaces such as other buildings, shading devices and even more distant objects (Evins et al., 2014). The radiation heat transfer from the cover surface to the sky depends on the sky temperature T_{sky} rather than the ambient temperature T_a. The sky can be considered as a blackbody at some equivalent T_{sky} to account for the fact that the atmosphere is not at a uniform temperature and that the atmosphere radiates only in a certain wavelength band (Duffie and Beckman, 1991). The simulation models help in addressing the challenges related to high costs of direct measurement of longwave radiation. With availability of hydro-meteorological data such as air temperature and relative humidity, longwave radiation can be estimated for any location and at any given time. But, most of the previous longwave radiation models are only valid for clear-sky or daytime conditions, while others are developed for daily or long-term predictions. Hence, these models are less accurate for estimation under cloudy conditions or within shorter time intervals (Iziomon et al., 2003). Therefore it is necessary to measure (and include into the models) atmospheric parameters such as cloudiness (Marty and Philipona, 2000). It is unclear from several studies how the atmospheric parameters affect the model sensitivities (Naud et al., 2013), especially in greenhouses. Therefore, this research work aims at modelling the longwave radiation exchange at exterior greenhouse surfaces under all-sky (clear-sky and overcast) conditions. The sensitivity of the longwave radiation models to the key parameters (air temperature, surface-to-air temperature difference, cloudiness and relative humidity) is also examined in this study.

2 Materials and methods

2.1 Experimental setup

An insulated thermal box (Figure 1) measuring 2.4 m long, 1.9 m wide and 1.2 m high was built to simulate the thermal radiation exchange of a greenhouse. The cover surface design (with a 4 mm normal single greenhouse float glass) was inclined at 26.5 °to the south and had a length of 2 m and a width of 1.5 m with steel glazing bars. The glass area was 86% while the area of all bars was 14% of the cover area. The base plate and the side walls were made from 0.2 m thick sandwich insulation panels (ESP 040, UNIDEK GEFINEX GmbH, Steinhagen, Germany). The inside and outside were covered with white lacquered aluminium sheets. The box had no transpiration systems inside, so it represented absolutely a dry greenhouse. Heating elements (800 W, Cr/Ni tubes, 6.9 mm diameter, 1.11 m length, and 2000 W, Cr/Ni tubes, 8.5 mm diameter and 1.11 m length) were used to provide heat sources inside the box. Due to this heating, the overall heat transfer coefficient (U_{cs}-value) measurement was possible using this system, but under a different study (Langner and Rath, 2014). The thermal box was placed outdoors at the Biosystems Engineering Section, Institute of Horticultural Production Systems, Leibniz Universität Hannover (52.39 °N, 9.706 ° E and altitude 52.3 m above mean sea level). This measurement site is located in Lower Saxony, which lies in the north of Germany.

Figure 1 Thermal box for thermal radiation exchange measurements

2.2 Data acquisition

The exterior surface temperatures of the glass and the glazing bars were measured with NTC-sensors (TS-NTC-104, Hygrosens, Germany). The sensors were glued to the glass and the glazing bar surfaces using a 2-component epoxy resin adhesive (UHU plus endfest 300, Bühl/Baden, Germany). The surrounding outside temperature and relative humidity were measured with a handheld psychrometer. The values were counterchecked with the meteorological weather data which were recorded at the university site.

Upward and downward facing thermal radiations were obtained with a newly acquired CNR 4 net radiometer (Kipp & Zonen, Delft, The Netherlands). The CNR 4 measures the energy that is received from the whole hemisphere (Kipp & Zonen, 2009). Additionally, four readily available 240-8110 net radiometers (NovaLynx Corporation, California, USA) were incorporated in order to obtain average net radiation values at the surface. The 240-8110 net radiometer model is an instrument for direct and instantaneous determination of net radiation in short and long wavelength range. To control the function and usage of the radiometers, occasional thermal surface inspection was done with the Varioscan 3022 thermal camera (Jenoptic Laser, Jena, Germany).

Data acquisition and control were done with the USB-Datalogger LabJack U12 (LabJack Corporation, Lakewood, USA), the signal amplifier LabJack EI-1040 (LabJack Corporation, Lakewood, USA) and the relay box ME-UBRE (Meilhaus Electronic GmbH, Alling, Germany). The ProfiLab Expert 4.0 software (ABACOM, Ganderkesee, Germany) was used to develop a comprehensive data logging system for both analogue measurements and digital controls. For the newly acquired CNR 4 net radiometer, the original calibration coefficients from the net radiometer company (Kipp & Zonen, Delft, The Netherlands) were used. For all other sensors standard calibration procedures were done before the measurements. The surface temperatures and the atmospheric parameters (air temperature and relative humidity) were measured during the months of January to April 2014 and recorded every 15 s. For the case of the radiation data, the time interval was large (frequency of 30 s) since some reasonable time was necessary for the concurrent data acquisition from the eight relays of ME-UBRE. All data were averaged to obtain the hourly means necessary to verify the longwave radiation estimations.

2.3 Mathematical modelling of longwave radiation exchange

Sky conditions were modelled on the basis of cloudiness factors *C*, which are very important parameters in longwave radiation exchange. The values were established using two approaches (Table 1). Firstly, the weather maps acquired from the web service Weather Online (www.wetteronline.de) were analyzed using a computer vision-based algorithm which was developed in Halcon 11.0 (HALCON 11.0.3, 2012). The algorithm identifies selected regions of interest on the maps and calculates the cloudiness situation at a given location, thus yielding a cloudiness factor C_{maps}. Secondly and for purposes of comparison, cloud covers in octas (eighths) were also obtained from the German Meteorological Service (www.dwd.de). The octas were assigned by experienced weather watchers. Based on these octa values (ranging from 0 to 8), a cloudiness factor C_{octas} was then attained. For both cases, hourly means were computed and used in the analysis.

Table 1 Parameterizations for clear-sky atmospheric emissivity suggested by different authors

Author	Equation	No.
Swinbank (1963)	$\varepsilon_{cs} = 9.365 \cdot 10^{-6} T_a^2$	(1)
Idso and Jackson (1969)	$\varepsilon_{cs} = 1 - 0.261 \exp\left\{-7.77 \cdot 10^{-4} (273 - T_a)^2\right\}$	(2)
Brutsaert (1975)	$\varepsilon_{cs} = 0.643 \left(\frac{e_a}{T_a}\right)^{1/7}$	(3)
Idso (1981)	$\varepsilon_{cs} = 0.70 + 5.95 \cdot 10^{-7} e_a \exp\left(\frac{1500}{T_a}\right)$	(4)
Sugita and Brutsaert (1993)	$\varepsilon_{cs} = 0.714 \left(\frac{e_a}{T_a}\right)^{0.0687}$	(5)
Prata (1996)	$\varepsilon_{cs} = 1 - \left(1 + 0.465 \frac{e_a}{T_a}\right) \exp\left\{-\left(1.2 + 1.395 \frac{e_a}{T_a}\right)^{0.5}\right\}$	(6)
Iziomon et al. (2003)	$\varepsilon_{cs} = 1 - X_s \exp\left(\frac{-Y_s e_a}{T_a}\right)$	(7)
Duarte et al. (2006)	$\varepsilon_{cs} = 0.625 \left(\frac{e_a}{T_a}\right)^{0.131}$	(8)
Kruk et al. (2010)	$\varepsilon_{cs} = 0.576 \left(\frac{e_a}{T_a}\right)^{0.202}$	(9)
Dos Santos et al. (2011)	$\varepsilon_{cs} = 0.6905 \left(\frac{e_a}{T_a}\right)^{0.0881}$	(10)

The effective atmospheric emissivity ε_a is often computed based on ground-based meteorological observations and is particularly a function of the cloudiness factor C and a basic clear-sky atmospheric emissivity ε_{cs} (Duarte et al., 2006). The ε_a is often applicable at the lower boundary of the atmosphere (Staley and Jurica, 1972). Since it is difficult to determine the bulk emissivity and the effective temperature of a vertical column of the atmosphere (Crawford and Duchon, 1999), parameterizations based on the screen level air temperature T_a and vapour pressure e_a are commonly used. Thus, the 10 commonly used parameterizations (Equation (1) to Equation (10)) were selected for the calculation of the clear-sky atmospheric emissivity (Table 1), where, ε_{cs} is the clear-sky atmospheric emissivity, e_a is the water vapour pressure of air, T_a is the air temperature, while X_s and Y_s are the site-dependent coefficients.

The values of the site-dependent coefficients X_s and Y_s in the algorithm of Iziomon et al. (2003) were extrapolated for the study location from the given values at lowland (212 m elevation) and mountain (1489 m elevation) sites. Considering the parameterizations for clear-sky atmospheric emissivity ε_{cs}, the X_s and Y_s values for the lowland site are 0.35 and 10 K/hPa respectively, while the corresponding values for the mountain site are 0.43 and 11.5 K/hPa (Iziomon et al., 2003). From the point of view of climatic characteristics, the variables

utilized in the ε_{cs} parameterizations showed a strong dependence on the site elevation.

The best ε_{cs} parameterization was chosen based on statistical criteria. The criteria included bias (BIAS), root mean square error (RMSE), mean absolute error (MAE), percentage mean root error (PMRE) and coefficient of determination (R^2). The ε_{cs} was used in the calculations of the effective atmospheric emissivity ε_a under all-sky (clear-sky and overcast) conditions. It has the basic structure (Duarte et al., 2006) as Equation (11):

$$\varepsilon_a = \varepsilon_{cs}\left(1 + b\,C^{\,d}\right) \qquad (11)$$

where, ε_{cs} is the clear-sky atmospheric emissivity, b and d are constants which can be determined experimentally, and C is the cloudiness factor. The locally calibrated values of b and d were found to be 0.24 and 0.58, respectively.

Another important parameter is the emissivity of surrounding ground objects ε_{gnd}. An emissivity ε_{gnd} of 0.97 was suggested by Howard and Stull (2013) particularly for tree temperatures ranging from -10 ℃ to 10 ℃. This value was used throughout this study, since a perfect blackbody is rare in nature (Petty, 2006).

The sky emissivity ε_{sky} is necessary in a quantitative understanding of the sky radiation. It can be approximated as a function of the dew point temperature (Chen et al., 1995), which is defined by the temperature and the relative humidity of air as Equation (12).

$$\varepsilon_{sky} = 0.732 + 0.0063\left\{T_o - \left(\frac{100 - RH}{5}\right)\right\} \qquad (12)$$

where, T_o is outside air temperature in ^{o}C and RH is relative humidity in %. The usual considered value of ε_{sky} is about 0.74 (Romila, 2012).

Also important is the emissivity of the cover surface ε_s, which includes glass and glazing bars. Emissivity values of 0.92 and 0.96 for glass and steel glazing bars were obtained from Fluke Corporation, respectively (Fluke, 2009).

A non-horizontal surface (e.g. roof and wall) does not radiate entirely to the whole sky and a view factor has to be used since this is less than one. The view factor is a purely geometrical parameter that accounts for the effects of orientation on radiation between the surfaces. The view factors to the sky F_{sky}, to the air F_{air} and to the ground F_{gnd} can be calculated as Equations (13), (14), (15), (16) and (17) (Romila, 2012; EnergyPlus 8.0, 2013):

$$F_{sky} = a\,F_s \qquad (13)$$

$$F_{air} = (1-a)\,F_s \qquad (14)$$

$$F_{gnd} = 1 - F_s = \sin^2\left(\frac{\beta}{2}\right) \qquad (15)$$

with,

$$F_s = \cos^2\left(\frac{\beta}{2}\right) \qquad (16)$$

$$a = \cos\left(\frac{\beta}{2}\right) \qquad (17)$$

where, a is the factor splitting the sky and air radiation and β is the surface inclination angle.

Apart from the measured surface temperature T_s, the ground temperature T_{gnd} was estimated from the air temperature (EnergyPlus 8.0, 2013). Modelling of longwave radiation exchange between the outside surfaces and the sky requires the knowledge of the sky temperature. The equivalent sky temperature T_{sky} has been estimated differently by various researchers. Some of the common equations (Equation (18) to Equation (21)) applied in T_{sky} computation are given in Table 2. These equations are empirical in nature and are related to the air temperature T_a. Thus, they perform best for areas with radiative climate similar to the one for which they were originally obtained. Hence, the available model (Equation 19) by von Elsner (1982) was selected since it was developed within the same study location. Other than air temperature, this model utilizes a cloudiness factor as an additional factor in T_{sky} estimation.

Table 2 Equations for the computation of the sky temperature

Author	Equation	No.
Tantau (1975)	$T_{sky} = T_a \left\{0.82 - 0.25 \cdot 10^{-0.095 P_d}\right\}^{1/4}$	(18)
Von Elsner (1982)	$T_{sky} = \left\{1.2\ T_o - 21.4 + C\left(20.6 - 0.26\ T_o\right)\right\} + 273.15$	(19)
Nijskens et al. (1984)	$T_{sky} = 0.0552\ T_a^{1.5}$	(20)
Duffie and Beckman (1991)	$T_{sky} = T_a \left\{0.711 + 0.0056\ T_d + 0.000073\ T_d^2 + 0.013 \cos\left(15\ \upsilon\right)\right\}^{1/4}$	(21)

Considering an exterior surface and the relevant parameters, the thermal radiation exchange of the surface Q_s (Equation (22)) is the sum of the components due to the exchange with the sky, the air and the ground.

$$Q_s = \varepsilon_s\ \sigma \left\{ \begin{array}{l} \varepsilon_{sky}\ F_{sky}\left(T_s^4 - T_{sky}^4\right) + \varepsilon_a\ F_{air}\left(T_s^4 - T_a^4\right) \\ + \varepsilon_a\ F_{gnd}\left(T_s^4 - T_{gnd}^4\right) \end{array} \right\} \quad (22)$$

where, σ is Stefan-Boltzmann constant (=5.67·10^{-8} W/m^{2}K^4)

Since the cover surface area is composed of 86% glass and 14% glazing bars with the respective emissivities and surface temperatures, the effective thermal radiation exchange $Q_{s,eff}$ was then calculated as Equation (23):

$$Q_{s,eff} = 0.86\ Q_{s,g} + 0.14\ Q_{s,gb} \quad (23)$$

where, $Q_{s,g}$ and $Q_{s,gb}$ are the thermal radiation exchange of the glass and the glazing bar surfaces, respectively. They are calculated with Equation (22) with ε_s and T_s for the glass surface or the glazing bar surface.

According to Rizou and Nnadi (2007), either air temperature or humidity parameters can capture all the downwelling longwave radiation LWR_d over a wide range of climatic conditions. This is because of the compensating effects of the temperature and the water vapour. For all-sky conditions, therefore, LWR_d has the general form (Choi et al., 2008; Dos Santos et al., 2011) as Equation (24):

$$LWR_d = \varepsilon_a\ \sigma\ T_a^4 \quad (24)$$

According to Howard and Stull (2013), longwave radiation from the surrounding objects such as trees can enhance the total downwelling longwave radiation $LWR_{d,t}$ and should not be neglected. This is specifically added for comparison with the measurement from the net radiometer. $LWR_{d,t}$ is therefore expressed as Equation (25):

$$LWR_{d,t} = LWR_d + \varepsilon_{gnd}\ F_{gnd}\ \sigma\ T_a^4 \quad (25)$$

An additional term accounting for the reflected downwelling radiation is incorporated in computation of the upwelling longwave radiation (Tang and Li, 2008). From the equations above, the sum of the emitted longwave radiation by the surface LWR_u and the reflected downwelling longwave radiation gives the total upwelling longwave radiation $LWR_{u,t}$ (Liang, 2004). The difference between all upwelling radiation and all downwelling radiation must result in $Q_{s,eff}$. Thus the $LWR_{u,t}$ is expressed in the form of Equation (26):

$$LWR_{u,t} = LWR_u + \left(1 - \varepsilon_s\right) LWR_d = Q_{s,eff} + LWR_d \quad (26)$$

2.4 Evaluation and sensitivity analysis of longwave radiation models

The calculations of this work were evaluated using the statistical standard criteria (BIAS, RMSE, MAE, PMRE and R^2). Sensitivity analysis for a number of

selected model parameters was done by a one-at-a-time (OAT) procedure. As the name suggests, the OAT approach allows only one parameter to vary each time, ignoring the effects of parameter interactions and multi-response interdependences (Saltelli et al., 2010). The atmospheric parameters considered for the OAT analysis included air temperature T_a, cloudiness factor C and relative humidity RH. Appropriate lower and upper boundaries (the feasible ranges) for the selected parameters were carefully derived based on the data acquired during the measurement period. The chosen range of T_a, C and RH were -20 ℃ to 20 ℃, 0 to 1 and 20% to 100%, respectively. To represent a heating situation, the surface-to-air temperature difference $\Delta T_{s\text{-}a}$ was subjectively set in the range of 0 ℃ to 16 ℃. The OAT analysis was done such that the longwave radiation model was run repeatedly for a number of times while varying a single parameter from the lower bound to the upper bound. A middle base value was selected within the feasible range each time while all the other parameters were fixed.

A dimensionless sensitivity index SI was calculated as the ratio between the relative change of the model output and the relative change of a parameter. According to Millington et al. (2009), SI can be computed as Equation (27):

$$SI = \frac{\Delta Y_{b,i} / Y_b}{\Delta X_{b,i} / X_b} \tag{27}$$

where, Y_b is the base value of the dependent variable (model output) and $\Delta Y_{b,i}$ is change in dependent output state variable Y_i from Y_b (i.e. Y_b-Y_i). Index b signifies the set base (in this case the median) while index i is the instantaneous model run being analyzed. X_b is the base value of parameter X (model parameter) and $\Delta X_{b,i}$ is the change in parameter X_i from the base value (i.e. X_b-X_i).

According to Lenhart et al. (2002), the calculated sensitivity indices can be assessed by ranking them into four classes (Table 3).

Table 3 Sensitivity classes for assessing sensitivity indices

Class	Sensitivity index SI (-)	Sensitivity
I	$0.00 \le \lvert SI \rvert < 0.05$	Small to negligible
II	$0.05 \le \lvert SI \rvert < 0.20$	Medium
III	$0.20 \le \lvert SI \rvert < 1.00$	High
IV	$\lvert SI \rvert \ge 1.00$	Very high

3 Results and discussion

3.1 Downwelling longwave radiation

Table 4 shows the comparative statistics for the performance of 10 clear-sky atmospheric emissivity calculation models both at night and during the day compared to the corresponding value computed directly from the measured data. Typical nights and days with mean hourly cloudiness of less than 1 octa (clear-sky) were used for the entire observation period. The performance of the models was ranked in ascending order based on the nighttime PMRE values with the best model at the top. During the nighttime, the best results were obtained by the Sugita and Brutsaert (1993) model, resulting in the smallest BIAS, RMSE, MAE and PMRE followed by the Ido and Jackson (1969) model. For daytime measurements, the results with the smallest BIAS, RMSE, MAE and PMRE were presented by the Sugita and Brutsaert (1993) model. The Kruk et al. (2010) model resulted in the highest errors under both night and day situations.

Table 4 Comparative statistics for the performance of clear-sky atmospheric emissivity calculation models for both nighttime and daytime measurements

Clear-sky atmospheric emissivity models	Nighttime measurements				Daytime measurements			
	BIAS (-)	RMSE (-)	MAE (-)	PMRE (%)	BIAS (-)	RMSE (-)	MAE (-)	PMRE (%)
Sugita and Brutsaert (1993)	0.000	0.011	0.009	1.174	-0.001	0.033	0.028	3.597
Idso and Jackson (1969)	-0.010	0.014	0.011	1.484	0.003	0.033	0.030	3.946
Prata (1996)	-0.010	0.015	0.012	1.648	-0.010	0.035	0.028	3.697
Dos Santos et al. (2011)	-0.014	0.018	0.016	2.085	-0.013	0.036	0.028	3.662
Iziomon et al. (2003)	-0.028	0.030	0.028	3.657	-0.028	0.043	0.034	4.301
Idso (1981)	0.032	0.034	0.032	4.265	0.021	0.040	0.036	4.787
Brutsaert (1975)	-0.037	0.039	0.037	4.897	-0.031	0.046	0.037	4.679
Swinbank (1963)	-0.053	0.054	0.053	7.033	-0.005	0.034	0.030	3.872
Duarte et al. (2006)	-0.063	0.064	0.063	8.351	-0.059	0.068	0.059	7.599
Kruk et al. (2010)	-0.083	0.084	0.083	11.067	-0.073	0.081	0.073	9.503

Comparisons between the simulated total downwelling longwave radiation ($LWR_{d,t}$) and the measured longwave radiation fluxes both at night and during the day are presented in Figure 2. The $LWR_{d,t}$ values varied in the range of about 255 W/m^2 to 400 W/m^2 and 260 W/m^2 to 430 W/m^2 for nighttime and daytime measurements, respectively. Due to the two approaches adopted for cloudiness predictions, the simulation was always in two datasets. It is noted from Figure 2(a) that a better model prediction was obtained for the nighttime observation period. In this case, simulation was based on the cloudiness factor from the analyzed weather maps C_{maps}. However, simulation with cloudiness factors derived from octas C_{octas} (assigned by the weather watcher) led to overestimation of $LWR_{d,t}$ during the day (Figure 2(b)).

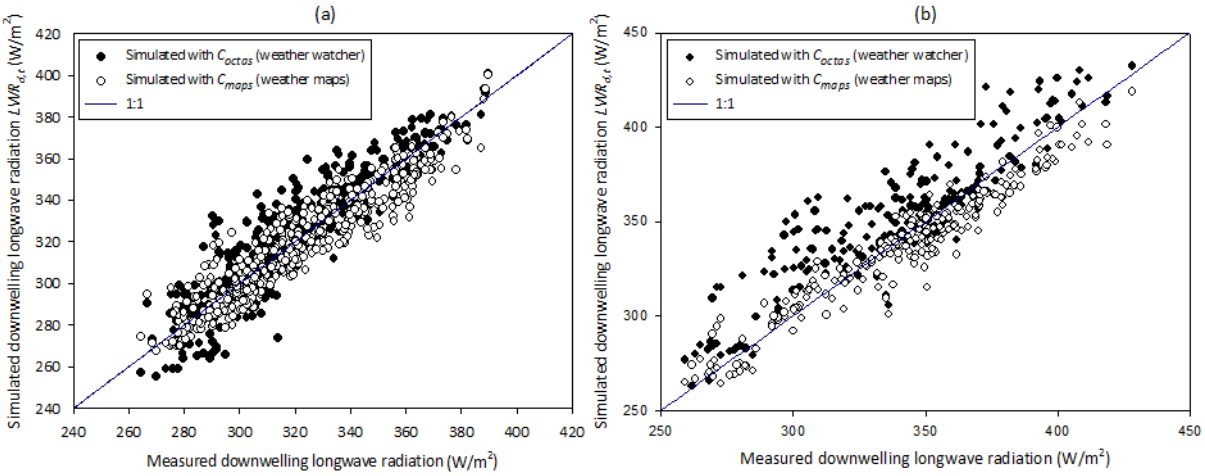

Figure 2 Comparison of simulated and measured downwelling longwave radiation: (a) nighttime and (b) daytime

In modelling of the downwelling longwave radiation LWR_d, the clear-sky atmospheric emissivity ε_{cs} parameterizations, which use water vapour pressure and air temperature, had the best scores. This confirms that the near-surface water vapour pressure is an important variable due to its impact as a greenhouse gas and should be applied in conjunction with the air temperature. Generally, the Sugita and Brutsaert model led to the best

results for both the daytime and the nighttime estimation of ε_{cs}. It requires only the air temperature and water vapour pressure measurements. The Duarte et al. (2006) and the Kruk et al. (2010) models underestimated the ε_{cs} values while the Idso (1981) model registered an overestimation of the ε_{cs}. Accurate estimation of the ε_{cs} directly influences the computation of the effective atmospheric emissivity. According to Ryu et al. (2008), LWR_d estimation becomes challenging because complex atmospheric components might affect atmospheric emissivity and could be the main reason of model uncertainties (Choi, 2013). Rizou and Nnadi (2007) pointed out that heterogeneous land cover types could affect atmospheric emissivity as well as air temperature and water vapour.

At night, longwave radiation is the sole source of radiant energy to the surface. During this time, the exterior surface exchanges longwave radiation with the sky, the ground and the surrounding elements. Other than solar radiation, longwave radiation exchanges also prevail during the day. The sum of the sky downwelling longwave radiation and the longwave radiation from the surrounding gives the total modelled downwelling longwave radiation $LWR_{d,t}$. This implies that integrated contributions from the entire upper hemisphere above the surface of interest are of concern while modelling. A similar observation was noted by Howard and Stull (2013) with the individual contributions of radiation being weighted by their view factors. The simulated $LWR_{d,t}$ values compared well with the measurements with the CNR 4 net radiometer. An additional component accounted for the longwave radiation from the surrounding ground objects adjacent to the measurement site. This agrees well with a behaviour noted by Howard and Stull (2013) while modelling the downwelling longwave radiation under clear skies. Although the work of Howard and Stull (2013) was applied on alpine ski racing (groomed ski run), the longwave radiation phenomena at the reference surface remain comparable.

3.2 Upwelling longwave radiation

The simulated total upwelling longwave radiation and the corresponding measured values are compared in Figure 3. Generally, the sum of the longwave radiation and the reflected downwelling radiation was in the range of about 300 W/m^2 to 430 W/m^2 at night and 280 W/m^2 to 490 W/m^2 during the day. At night, heating of the developed thermal box system increased the surface temperatures, thereby the total upwelling longwave radiation $LWR_{u,t}$ was increased. Despite no heating of the developed system during daytime, the $LWR_{u,t}$ values were equally high due to solar radiation presence.

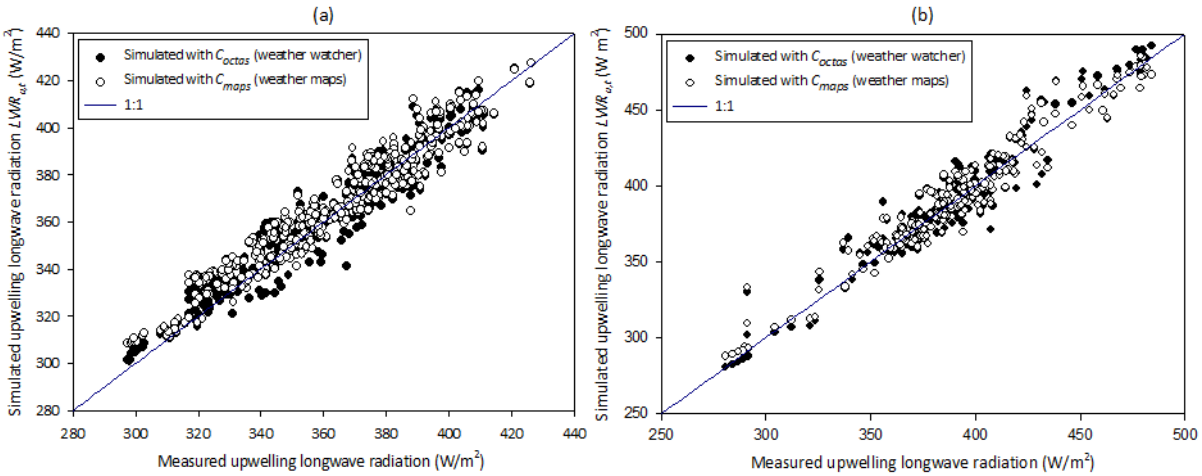

Figure 3 Comparison of simulated and measured upwelling longwave radiation: (a) nighttime and (b) daytime

With precise computation of the effective thermal radiation exchange $Q_{s,eff}$ and the reflected component of atmospheric downwelling longwave radiation LWR_d, the upwelling longwave radiation $LWR_{u,t}$ can then be

obtained (Ronoh and Rath, 2014). The effective surface temperature $T_{s,eff}$ (for glass and glazing bars) and the surface emissivity strongly influence the output of $LWR_{u,t}$. To a certain degree, vegetation influences the $LWR_{u,t}$ since thick vegetation cover can act to retard the radiation emitted from the ground via multiple reflections.

3.3 Model evaluation and sensitivity analysis

Table 5 shows the comparison of nighttime and daytime comparative statistics for the performance of the longwave radiation models. For both downwelling and upwelling longwave radiation models, the simulation was done with the two cloudiness prediction approaches (weather watcher and analyzed weather maps). In both cases, better estimation was obtained through simulation with cloudiness factors obtained from the vision-based analysis of weather maps. Low values of BIAS, RMSE, MAE and PMRE, and high R^2 led to best results in terms of model prediction. However, simulation with the two cloudiness estimation methods yielded results which were not significantly different ($p > 0.05$).

Table 5 Comparative statistics for the performance of longwave radiation models under both night and day situations

	Nighttime measurements					Daytime measurements				
Model*	BIAS (W/m^2)	RMSE (W/m^2)	MAE (W/m^2)	PMRE (%)	R^2 (-)	BIAS (W/m^2)	RMSE (W/m^2)	MAE (W/m^2)	PMRE (%)	R^2 (-)
$^cLWR_{d,t}$	2.362	11.011	8.296	2.632	0.870	11.801	19.765	14.766	4.536	0.818
$^dLWR_{d,t}$	-3.810	9.188	7.353	2.284	0.910	-4.477	11.322	9.022	2.643	0.929
$^cLWR_{u,t}$	0.266	8.017	6.246	1.730	0.912	1.761	11.449	8.713	2.231	0.924
$^dLWR_{u,t}$	2.153	7.843	6.411	1.796	0.924	1.523	10.199	7.751	2.004	0.935

Note: *Simulated with: ^{c}cloudiness factor C_{octas} (weather watcher), ^{d}cloudiness factor C_{maps} (weather maps).

Based on the variation of the key parameters from the base value (median), temperature clearly stands out to be the critical parameter influencing the longwave radiation models (Figure 4). Considering air temperature T_a change of 45 K, the increment in $LWR_{d,t}$ was as high as 115.35%. The $LWR_{d,t}$ fluxes increased by about 22.6% under cloudy conditions (cloudiness factor C = 1) while for 60% change in relative humidity RH, the increment in $LWR_{d,t}$ was only 11%. Clouds seemed to be more sensitive in the effective thermal radiation exchange $Q_{s,eff}$ model than in the $LWR_{d,t}$ model, but generally T_a and the surface-to-air temperature difference ΔT_{s-a} were the most sensitive parameters.

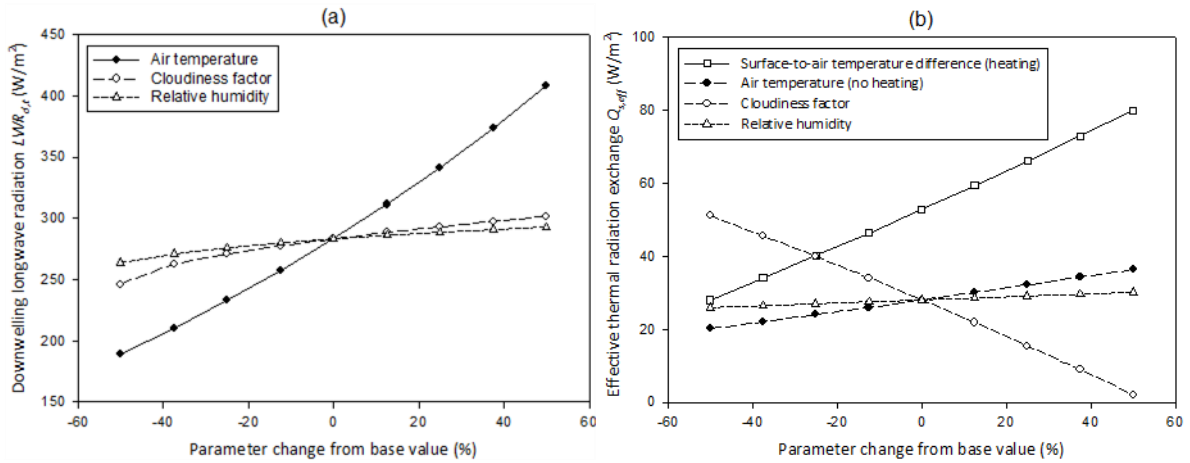

Figure 4 Sensitivity of longwave radiation models to changes in the key parameters (T_a, C, RH and ΔT_{s-a}): (a) downwelling longwave radiation and (b) effective thermal radiation exchange

The sensitivity indices obtained from the sensitivity analysis of the longwave radiation models are presented in Table 6. For the $LWR_{d,t}$ model, the highest sensitivity index *SI* was due to changes in air temperature. Changes in both cloudiness and relative humidity resulted in low *SI* values, with the latter registering the lowest. Similar results were noted for the case of $Q_{s,eff}$ model. The highly sensitive parameter still stands out to be temperature. However, the higher *SI* was as a result of the increment in the temperature difference between the surface and the air. The sensitivity indices due to changes in cloudiness and relative humidity in the q_{lw} model were high and medium, respectively.

Table 6 Sensitivity indices of longwave radiation models due to parameter changes

Model output variable	Sensitivity index *SI* of the model based on key parameters			
	Air temperature	Cloudiness factor	Relative humidity	Temperature difference
	T_a (K)	C (-)	RH (%)	$\Delta T_{s\text{-}a}$ (K)
Downwelling longwave radiation $LWR_{d,t}$ (W/m^2)	5.241	0.084	0.07	-
Effective thermal radiation exchange $Q_{s,eff}$ (W/m^2)	10.201[e]	0.872	0.112	17.224[f]

Note: ([e] with no heating; [f] with heating)

The downwelling longwave radiation varies with air temperature, cloudiness and relative humidity. The trend (see Figure 4) attests to the fact that T_a is the major factor in the model. Additionally, the sensitivity index *SI* of T_a is greater than one while for the parameters *C* and *RH*, the $SI < 0.2$. This also explains the fact that errors related to longwave radiation simulation with the two cloudiness approaches (values from the weather watcher and the analyzed weather maps) are not significantly different ($p > 0.05$). The higher the *SI*, the higher the model sensitivity due to changes in that parameter. The *C* parameter appears to be more sensitive in the $Q_{s,eff}$ model ($SI > 0.2$) than in the $LWR_{d,t}$ model ($SI < 0.2$). Although clouds reflect some downward radiation back to space, they also reradiate infrared energy back towards the earth's surface. This implies that clouds increase the longwave radiation to the surface, thereby enhancing the net cooling effect in the daytime but a net warming at night. These factors (T_a, *C* and *RH*) are interrelated and they jointly influence the radiation model output. Overall, T_a and the surface-to-air temperature difference ($\Delta T_{s\text{-}a}$) are the key parameters in the $LWR_{d,t}$ and $Q_{s,eff}$ models, respectively (see Table 6). This is in agreement with the Stefan-Boltzmann law where the rate of longwave energy emission is proportional to the absolute temperature of the surface raised to the fourth power.

4 Conclusions

From the present study, the findings demonstrate that the prediction models provide a more realistic understanding of the longwave radiation exchange between the greenhouse surfaces and the sky if all the required parameters are accurately determined. The clear-sky atmospheric emissivity parameterizations that include both the near-surface water vapour pressure and the air temperature tend to outperform those consisting of only the air temperature. Under both day and night situations, the study delivers reliable results in terms of calculation of parameters necessary for the longwave radiation models. However, it is important to evaluate locally adjusted equations to estimate some of the model parameters. In general, the longwave radiation exchange between surfaces is generally dependent on surface temperatures, spatial relationships between these surfaces and their surroundings, and the relevant material properties of the surfaces. At the greenhouse surfaces, it has been shown that the weighted contributions of thermal emissions from the ground, the sky and the surrounding air are explained by the view factors. The

inclusion of cloudiness prediction, through octa given by the weather watchers and through a computer-based analysis of weather maps, provides an appreciable improvement on the prediction models.

It is critical also to explore how the sensitivity of the longwave radiation models is affected due to changes in the key parameters. A sensitivity index *SI* allows better understanding of these parameters in a simulation model. For both the total downwelling longwave radiation $LWR_{d,t}$ and the effective thermal radiation exchange $Q_{s,eff}$ models, air temperature was the most sensitive parameter ($SI > 1$) while relative humidity was the least sensitive ($SI < 0.2$). Cloudiness, however, turned out to be more sensitive in the $Q_{s,eff}$ model ($0.2 < SI < 1$) than in the $LWR_{d,t}$ model ($SI < 0.2$). Further work will consider a possibility to establish the significance of the radiative heat transfer at the exterior greenhouse surfaces in the overall heat transfer coefficient (U_{cs}-value).

Acknowledgements

The joint scholarship support (National Commission for Science, Technology and Innovation (NACOSTI), Kenya and German Academic Exchange Service (DAAD), Germany) provided to the first author is highly acknowledged.

References

Brutsaert, W. 1975. On a derivable formula for long-wave radiation from clear skies. *Water Resources Research*, 11(5): 742-744.

Chen, B., D. Clark, J. Maloney, W. N. Mei, and J. Kasher. 1995. Measurements of night sky emissivity in determining radiant cooling from cool storage roofs and roofs ponds. In: *Proceedings of American Solar Energy Society*. *Annual Meeting*, Minneapolis, USA.

Choi, M. 2013. Parameterizing daytime downward longwave radiation in two Korean regional flux monitoring network sites. *Journal of Hydrology*, 476(1): 257-264.

Choi, M., J. M. Jacobs, and W. P. Kustas. 2008. Assessment of clear and cloudy sky parameterizations for daily downwelling longwave radiation over different land surfaces in Florida, USA. *Geophysical Research Letters*, 35(L20402): 1-6.

Crawford, T. M., and C. E. Duchon. 1999. An improved parameterization for estimating effective atmospheric emissivity for use in calculating daytime downwelling longwave radiation. *Journal of Applied Meteorology*, 38(4): 474-480.

Dos Santos, C. A. C., B. B. Da Silva, T. V. R. Rao, P. Satyamurty, and A. O. Manzi. 2011. Downward longwave radiation estimates for clear-sky conditions over northeast Brazil. *Revista Brasileira de Meteorologia*, 26(3): 443-450.

Duarte, H. F., N. L. Dias, and S. R. Maggiotto. 2006. Assessing daytime downward longwave radiation estimates for clear and cloudy skies in southern Brazil. *Agricultural and Forest Meteorology*, 139(3-4): 171-181.

Duffie, J. A., and W. A. Beckman. 1991. *Solar engineering of thermal processes*. New York, USA: John Wiley & Sons, Inc.

EnergyPlus 8.0. 2013. Engineering reference: Outside surface heat balance. Available at: http://bigladdersoftware.com/epx/docs/8-0/engineering-reference. Accessed 20 September 2013.

Evins, R., V. Dorer, and J. Carmeliet. 2014. Simulating external longwave radiation exchange for buildings. *Energy and Buildings*, 75: 472-482.

Fluke. 2009. Emissivity values of common materials. Everett, WA, USA: Fluke Corporation. Available at: http://www.fluke.com. Accessed 14 April 2013.

German Weather Service (Deutscher Wetterdienst, DWD). Web weather request and distribution system (WebWerdis). Available at: http://www.dwd.de. Accessed 9 July 2013.

HALCON Version 11.0.3. 2012. *HALCON/HDevelop Reference Manual*. München, Germany: MVTec Software GmbH.

Howard, R., and R. Stull. 2013. Modeling the downwelling longwave radiation over a groomed ski run under clear skies. *Journal of Applied Meteorology and Climatology*, 52(7): 1540-1553.

Idso, S. B. 1981. A set of equations for full spectrum and 8 to 14 μm and 10.5 to 12.5 μm thermal radiation from cloudless skies. *Water Resources Research*, 17(2): 295-304.

Idso, S. B., and R. D. Jackson. 1969. Thermal radiation from the atmosphere. *Journal of Geophysical Research*, 74(23): 5397-5403.

Iziomon, M. G., H. Mayer, and A. Matzarakis. 2003. Downward atmospheric longwave irradiance under clear and cloudy skies: measurement and parameterization. *Journal of Atmospheric and Solar-Terrestrial Physics*, 65(10): 1107-1116.

Kipp & Zonen. 2009. *Instruction manual, CNR 4 net radiometer*. Manual version 1107. Delft, The Netherlands.

Kruk, N. S., I. F. Vendrame, H. R. Rocha, S. C. Chou, and O. Cabral. 2010. Downward longwave radiation estimates for clear and all-sky conditions in the Sertãozinho region of São Paulo, Brazil. *Theoretical and Applied Climatology*, 99(1-2): 115-123.

Langner, F., and T. Rath. 2014. Entwicklung eines differenzierten Widerstandsmodells zur Erstellung vergleichbarer Energiebedarfsberechnung von Gewächshäusern (Development of a differentiated resistance model for a comparable calculation of greenhouse energy demands). *DGG & BHGL 49th Horticultural Science Conference*, BHGL Tagungsband 30, p. 27. Dresden, Germany, 5–8 March.

Lenhart, T., K. Eckhardt, N. Fohrer, and H. -G. Frede. 2002. Comparison of two different approaches of sensitivity analysis. *Physics and Chemistry of the Earth*, 27(9-10): 645-654.

Liang, S. L. 2004. *Quantitative remote sensing of land surfaces*. New Jersey, USA: John Wiley & Sons.

Marty, C., and R. Philipona. 2000. The clear-sky index to separate clear-sky from cloudy-sky situations in climate research. *Geophys. Res. Lett.*, 27(17): 2649-2652.

Millington, J., J. Wainwright, G. L. Perry, R. Romero-Calcerrada, and B. D. Malamud. 2009. Modelling Mediterranean landscape succession-disturbance dynamics: A landscape fire-succession model. *Environmental Modelling and Software*, 24(10): 1196-1208.

Naud, C. N., Y. Chen, I. Rangwala, and J. R. Miller. 2013. Sensitivity of downward longwave surface radiation to moisture and cloud changes in a high-elevation region. *Journal of Geophysical Research: Atmospheres*, 118(17): 10072-10081.

Nijskens, J., J. Deltour, S. Coutisse, and A. Nisen. 1984. Heat transfer through covering materials of greenhouses. *Agricultural and Forest Meteorology*, 33(2-3): 193-214.

Petty, G. W. 2006. *A first course in atmospheric radiation*. WI, 2nd Edition, 459, Madison: Sundog Publishing.

Prata, A. J. 1996. A new long-wave formula for estimating downward clear-sky radiation at the surface. *Quarterly Journal of the Royal Meteorological Society*, 122(533): 1127-1151.

Rizou, M., and F. Nnadi. 2007. Land use feedback on clear sky downward longwave radiation: A land use adapted model. *International Journal of Climatology*, 27(11): 1479-1496.

Romila, C. 2012. Night radiation effect on energy performance of ventilated facades. *Bulletin of the Polytechnic Institute of Jassy (Construction, Architecture Section)*, 58(62): 21-28.

Ronoh, E. K., and T. Rath. 2014. Investigations on the external thermal radiation exchanges between the glass-covered greenhouse surfaces and the sky. *DGG-Proceedings*, 4(6): 1-5.

Ryu, Y., S. Kang, S. K. Moon, and J. Kim. 2008. Evaluation of land surface radiation balance derived from moderate resolution imaging spectroradiometer (MODIS) over complex terrain and heterogeneous landscape on clear sky days. *Agricultural and Forest Meteorology*, 148(10): 1538-1552.

Saltelli, A., P. Annoni, I. Azzini, F. Campolongo, M. Ratto, and S. Tarantola. 2010. Variance based sensitivity analysis of model output: Design and estimator for the total sensitivity index. *Computer Physics Communications*, 181(2): 259-270.

Staley, D. O., and G. M. Jurica. 1972. Effective atmospheric emissivity under clear skies. *Journal of Applied Meteorology*, 11(2): 349-356.

Sugita, M., and W. Brutsaert. 1993. Cloud effect in the estimation of instantaneous downward longwave radiation. *Water Resources Research*, 29(3): 599-605.

Swinbank, W. C. 1963. Long-wave radiation from clear skies. *Quarterly Journal of the Royal Meteorological Society*, 89(381): 339-348.

Tang, B. H., and Z. L. Li. 2008. Estimation of instantaneous net surface longwave radiation from MODIS cloud-free data. *Remote Sensing of Environment*, 112(9): 3482-3492.

Von Elsner, B. 1982. Das Kleinklima und der Wärmeverbrauch von geschlossenen Gewächshäusern: Ein Simulationsmodell zur gartenbautechnischen Bewertung unter Berücksichtigung des Einflusses von Standortklima, Pflanzenbestand und Gewächshauskonstruktion (The microclimate and heat consumption of closed greenhouses: A simulation model taking local climate, plants and greenhouse construction into account). Dissertation, *Gartenbautechnische Informationen*, Heft 12, Institut für Technik in Gartenbau und Landwirtschaft, Universität Hannover, Germany.

Weather Online (WetterOnline). Weather maps - clouds, rain and snow at a glance. Available at: http://www.wetteronline.de. Accessed 9 July 2013.